Technical Note

In Vitro Validation of Flow Measurement With Phase Contrast MRI at 3 Tesla Using Stereoscopic Particle Image Velocimetry and Stereoscopic Particle Image Velocimetry-Based Computational Fluid Dynamics

Iman Khodarahmi, MD, PhD,[1] Mostafa Shakeri, PhD,[1] Melanie Kotys-Traughber, PhD,[2] Stefan Fischer, PhD,[2] M. Keith Sharp, PhD,[3] and Amir A. Amini, PhD[1]*

Purpose: To validate conventional phase-contrast MRI (PC-MRI) measurements of steady and pulsatile flows through stenotic phantoms with various degrees of narrowing at Reynolds numbers mimicking flows in the human iliac artery using stereoscopic particle image velocimetry (SPIV) as gold standard.

Materials and Methods: A series of detailed experiments are reported for validation of MR measurements of steady and pulsatile flows with SPIV and CFD on three different stenotic models with 50%, 74%, and 87% area occlusions at three sites: two diameters proximal to the stenosis, at the throat, and two diameters distal to the stenosis.

Results: Agreement between conventional spin-warp PC-MRI with Cartesian read-out and SPIV was demonstrated for both steady and pulsatile flows with mean Reynolds numbers of 130, 160, and 190 at the inlet by evaluating the linear regression between the two methods. The analysis revealed a correlation coefficient of >0.99 and >0.96 for steady and pulsatile flows, respectively. Additionally, it was found that the most accurate measures of flow by the sequence were at the throat of the stenosis (error $<5\%$ for both steady and pulsatile mean flows). The flow rate error distal to the stenosis was primarily found to be a function of narrowing severity including dependence on proper Venc selection.

Conclusion: SPIV and CFD provide excellent approaches to in vitro validation of new or existing PC-MRI flow measurement techniques.

Key Words: phase contrast MRI; pulsatile flow; stenosis; particle image velocimetry; computational fluid dynamics
J. Magn. Reson. Imaging 2014;39:1477–1485.

PHASE-CONTRAST MRI (PC-MRI) provides a powerful and noninvasive method for the quantification of blood velocity (1,2). The major advantage of MR velocity measurement is its unique ability to measure all three orthogonal components of the velocity vector in an imaging slice. The velocity field can then be used to derive other clinically useful hemodynamic parameters, such as wall shear stress and blood pressure gradient (3–5). PC-MRI has been applied in several clinical scenarios, such as evaluation of aortic coarctation and dissection, valvular heart abnormalities, peripheral arterial diseases, and congenital shunt lesions, as well as quantification of cardiac function (6).

Quantitative measurements of PC-MRI have been validated by several other velocity/flow measurement techniques, the simplest being the fluid collection method (7,8). Doppler ultrasound has also been used as a reference technique for both in vitro and in vivo flow measurements. However, ultrasound suffers from the inherent problem of only being able to measure flow velocities in the direction of insonification, which may have contributed to the mixed correlations with PC-MRI observed across several studies (9–13).

Electromagnetic flow meters have also been applied to measure the steady flow rate in a few studies (14,15). Although this technique is more accurate for steady flows, it suffers from lack of sufficient accuracy for pulsating flows.

Alternative methods such as laser Doppler velocimetry (LDV) have been used to evaluate the accuracy of

[1]Medical Imaging Lab, Department of Electrical and Computer Engineering, University of Louisville, Louisville, Kentucky, USA.
[2]Philips Healthcare, Cleveland, Ohio, USA.
[3]Department of Mechanical Engineering, University of Louisville, Louisville, Kentucky, USA.
Contract grant sponsor: National Science Foundation; Contract grant number: 0730467; Contract grant sponsor: the Clinical and Translational Research Program of the University of Louisville, A. Amini, PI.
*Address reprint requests to: A.A.A., Medical Imaging Laboratory, Department of Electrical and Computer Engineering, 409 Lutz Hall, University of Louisville, Louisville, KY 40292. E-mail: amir.amini@louisville.edu
Received November 11, 2011; Accepted June 25, 2013
DOI 10.1002/jmri.24322.
View this article online at wileyonlinelibrary.com.

PC-MRI. Steady flows in straight, stenotic, and aneurysmal models (16–18) and pulsatile flows in aneurysmal models (19) revealed a wide range of accuracy for PC-MRI using LDV for validation. LDV is a well-established method for analyzing particle movement at a "single point" in the fluid based on the Doppler effect. The LDV point measurement technique, however, requires a significant amount of time to delineate a three-dimensional (3D) velocity field.

In contrast to single point measurement techniques, particle image velocimetry (PIV) can concurrently acquire 2D velocity information across an entire plane making it possible to detect in-plane 2D flow structures with excellent spatial and temporal resolution. Previous studies have compared PC-MRI against PIV for velocity comparison in phantom models of congenital heart diseases (20) and intracranial aneurysms (21).

Stereoscopic PIV (SPIV), using two cameras rather than one, provides all three components of the velocity vector. Consequently, SPIV can serve as a reliable reference standard for validation of in vitro PC-MRI measurements in complicated geometries where other velocity measurement techniques cannot be easily applied.

In this study, we used a SPIV system as gold standard for validation of MRI measurements of steady and pulsatile flows through stenotic phantoms with various degrees of narrowing at Reynolds numbers mimicking flows in the human iliac artery.

MATERIALS AND METHODS

Flow System

All experiments were carried out using a closed flow system (Fig. 1a). A MR compatible, computer controlled pump (CardioFlow 1000 MR, Shelley Medical Imaging Technologies, London, Ontario, Canada) was used with the capability to generate user-provided flow waveforms.

Idealized rigid models of axisymmetric Gaussian shape were machined from transparent acrylic, initially specified at 50%, 75%, and 90% area occlusion (Fig. 1b). Later, the exact geometry was measured with high resolution computed tomography (CT) scans ($0.22 \times 0.22 \times 0.625$ mm^3) and the area occlusions were found to be 50%, 74%, and 87%, respectively. The inlet diameter for all three models was 25.4 mm. To ensure fully developed laminar flow at the entrance of the model, a 75-cm-long straight rigid acrylic tube was placed upstream of the test section. A solution of glycerol and water (60:40, w/w) was prepared and then sodium iodide was added to match its refractive index to that of acrylic ($n = 1.494$) to minimize errors due to refraction. Finally, neutrally buoyant fluorescent polymer spheres with mean diameter of 10 μm were added to the fluid as seeding particles for SPIV measurements. The final density and viscosity of the solution were 1600 kg/m^3 and 0.022 Pa·s, respectively, at 68°F, compared with the corresponding values of 1060 kg/m^3 and 0.0035 Pa·s for the blood. The T1 and T2 values of the final solution were 500 and 45 ms, respectively, at 3 T.

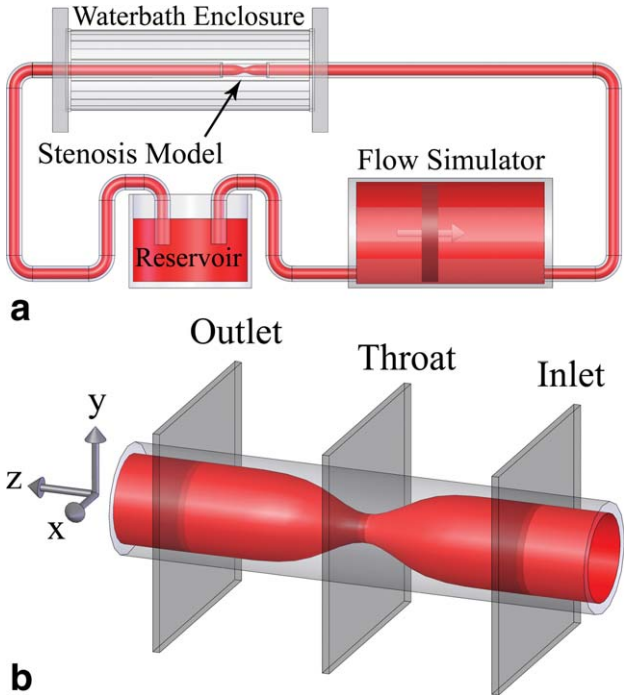

Figure 1. a: Schematic diagram of the flow apparatus. **b:** Three different imaging planes for MR imaging: inlet (two diameters proximal to the throat), throat and outlet (two diameters distal to the throat).

Flow Regimes

For steady flows, inlet Reynolds numbers (Re) of 190, 160, and 130 corresponding to the range of Reynolds number typically encountered in the human common iliac artery (mean ± 20%) were used. We chose to model flow in the human common iliac artery because it is one of the most common sites for development of atherosclerotic lesions. Another steady flow with inlet Reynolds number of 550 (mimicking the human renal artery) was used to study the validity of conventional PC-MRI at high velocities (Table 1).

In addition to steady flows, three biphasic pulsatile flows with the same mean Reynolds numbers (i.e., 190, 160, and 130) with peak Reynolds number of 360, 300, and 250 were also studied (Table 1). At a frequency of 60 beats/min, the Womersley number was 8.6, similar to that in the human common iliac artery. By matching both the Reynolds and the Womersley numbers to those of human iliac artery, it is ensured that the flow behaves physiologically, irrespective of the diameter of the phantom. We note however that in-vivo flow in a human common iliac artery has a negative diastolic component which our in-vitro system is unable to recreate.

PC-MRI Experiments

All PC-MRI experiments were conducted on an Achieva 3T TX MRI scanner (Philips Healthcare, Best, Netherlands) with a maximum gradient strength of 80 mT/m and a maximum slew rate of 200 T/m/s using a multichannel knee coil. A conventional 2D phase contrast sequence with Cartesian read-out, through-

Table 1
Steady and Pulsatile Flow Cases With Corresponding Reynolds Numbers (Re)

Steady flows			Pulsatile flows, Womersley number 8.6			
Steady flow	Flow rate (ml/s)/ Venc (cm/s)	Inlet Re	Pulsatile flow	Mean inlet flow rate (ml/s)/Venc (cm/s)	Mean inlet Re	Peak inlet Re
SF-0	150/75	550				
SF-1	53/30	190	PF-1	53/40	190	360
SF-2	44/30	160	PF-2	44/40	160	300
SF-3	35/30	130	PF-3	35/40	130	250

plane velocity encoding, and velocity compensation in all three directions was used to image three different sections perpendicular to the long axis of the phantom: two diameters proximal to the stenosis (hereafter called the inlet), at the throat, and two diameters distal to the stenosis (hereafter called the outlet, Fig. 1b). The throat of the stenosis was placed at the iso-center of the magnet, with the long axis of the phantom parallel to the B_0 magnetic field.

Imaging parameters were as follows: TE/TR = 3.0/4.0 ms, slice-thickness = 4 mm, flip angle = 20°, Field of view = 64 × 64 mm, Resolution = 1 × 1 mm, and velocity encoding (V_{enc}) = 30–120 cm/s for steady flows and 50–200 cm/s for pulsatile flows, depending on the flow and imaging section. To avoid aliasing while providing maximum sensitivity for each section, for steady flows of Re = 550 (SF-0) and Re = 190 (SF-1), and pulsatile flow phantom of Re = 190 (PF-1), V_{enc} was chosen to be roughly 10–20% above the expected peak velocity. To evaluate the importance of proper V_{enc} selection, the V_{enc} prescribed for SF-1 was also used for steady flows of Re = 160 (SF-2) and Re = 130 (SF-3); and the one prescribed for PF-1 was also used for pulsatile flows of Re = 160 (PF-2) and Re = 130 (PF-3). Number of signal averages, NEX, was set to 10 and to 2 for steady and pulsatile flows, respectively. The ECG trigger for the pump with a frequency of 1 Hz was used to retrospectively gate for 40 cardiac phase acquisitions, corresponding to a temporal resolution of 25 ms for pulsatile flows.

All PC velocity images were corrected for background phase errors resulting from Maxwell's concomitant gradient terms and eddy currents. To do this, first degree polynomials were fitted to no flow images collected with the pump turned off, at the same locations and with the same imaging parameters. Later, the resulting polynomial surface fits were subtracted from the corresponding velocity images.

To remove flow calculation errors due to variations in the area, a region of interest on every slice was defined using a circular mask at phantom contours defined from high resolution CT images. To minimize partial volume errors, the resolution of MR velocity images was artificially increased to that of CT images using nearest-neighbor interpolation before fitting a circular mask. Subsequently, individual pixels which had more than 50% of their area contained within the contour were included in the mask. All of the aforementioned analyses as well as flow calculation from MRI data were performed within a software environment written in MATLAB (The MathWorks, Natick, MA, USA).

Stereoscopic-PIV Measurements

A stereoscopic PIV system (TSI, Inc., MN) was used to measure velocity vectors in the cross-section of the phantom model proximal to the stenosis (Fig. 2). The same experimental conditions with identical phantoms and flow connectors were used in SPIV measurements to ensure reproducibility of flow conditions between MRI and SPIV studies. The SPIV system included two Nd-YAG lasers and two high-resolution digital cameras pointed at the laser sheet at 45° angles. The laser light sheet illuminated a vertical plane in the flow perpendicular to the flow direction. More details about the experimental setup may be found in (23,24). For each camera, two consecutive images with a temporal resolution of 80–1200 μs (depending on the flow regimen) were captured and the fluid velocity was extracted using a cross-correlation scheme. The field of view of each camera (after dewarping) was approximately 50 mm × 27 mm

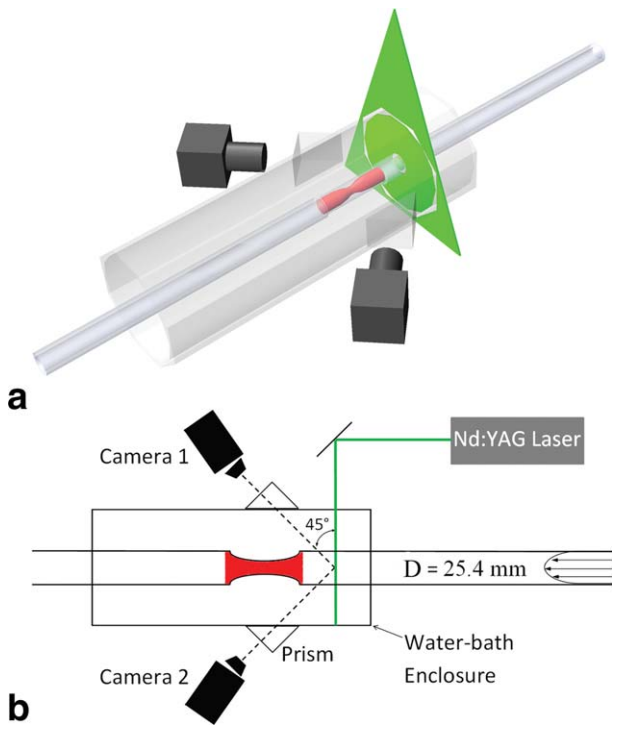

Figure 2. Isometric view (**a**) and schematic top view (**b**) of the SPIV apparatus for flow measurement showing the laser sheet (green) and two digital cameras (black) viewing the intersection of the stenosis (red) with the laser sheet at 45°. Flow direction is from right to left.

yielding a nominal spatial resolution of 205 μm for the velocity data points. To reduce optical refraction mismatches between the fluid and acrylic, the stenosis model was immersed in a water-bath enclosure (length = 24 in, diameter = 8 in) with flat windows and filled with the same fluid used inside the loop. Also, two 45° prisms were built from transparent acrylic, filled with the same fluid in the water-bath enclosure, and placed in front of each camera to make the optical axis of the cameras perpendicular to the viewing window (Fig. 2).

Each camera used consecutive images to measure displacement of the seeding particles perpendicular to its viewing angle. The displacement over the time between images provided estimates of velocity. These two different projections of the velocity, one from each camera, can be combined to reconstruct the three components of velocities. In practice, the two-component particle displacement fields observed by each camera were first evaluated by standard PIV cross-correlation methods. Subsequently, the particle displacement fields were mapped (dewarped) from the image planes onto the real-world plane of the light sheet and interpolated on a rectangular grid. Finally, the displacement vectors from both cameras were combined to reconstruct the three components of particle displacements based on a calibration procedure (25).

To improve accuracy, each spatial velocimetry assessment was generated through averaging results from 30 pairs of images for steady flows and 12 pairs of images for pulsatile flows, therefore providing more robust velocity estimation and overcoming possible artifacts like small equipment vibrations, transient bubble passages, or slight flow variations. The temporal resolution of pulsatile flow measurements was 25 ms, corresponding to 40 measurements per second.

SPIV measurements were performed only at the inlet to evaluate bulk flow, which is constant along the rigid phantom. In our case, SPIV technique was not possible for the throat and outlet sections due to difficulties in the fabrication of an optically clear phantom; however, the SPIV method in general could be applied to any optically clear plane of interest. Instead, to spatially localize the observed errors in the flow, computational fluid dynamics (CFD) simulations of the flow were performed for identical cross sections.

CFD Simulations

The flow was numerically simulated for the same flow conditions. The exact geometry obtained from the high resolution CT data was imported to the mesh generation preprocessor, GAMBIT 2.4.6 (ANSYS, Inc., Canonsburg, PA) and a nonuniform mesh with higher density at the throat and near-the-wall was created. To ensure adequate resolution, a finer mesh with twice the node density was also generated. Differences between the velocity fields computed on the two meshes were negligible, verifying mesh independence of the numerical solution. The finer mesh with more than 1,200,000 pyramid/wedge-shaped computational cells was used for all simulation results presented here.

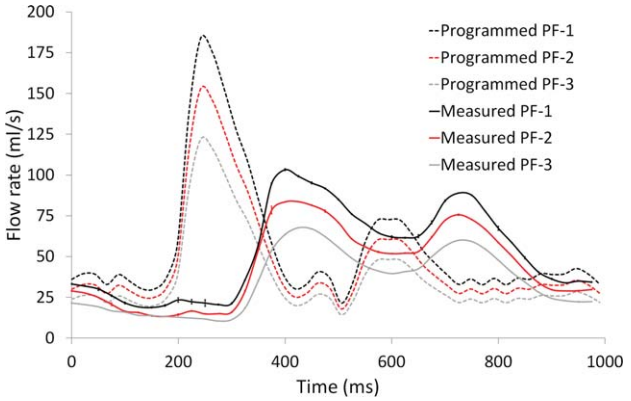

Figure 3. Programmed and measured flow waveforms. Dashed curves are applied by the computer controlled pump and solid curves are the measured flow using SPIV, each curve with 40 point measurements. Error bars on the measured flow waveforms show the standard deviation of the SPIV measurements.

Velocity distribution over the phantom volume was computed by solving the 3D Navier-Stokes equations for an incompressible Newtonian fluid, with rigid walls using the CFD software package Fluent 12.1 (ANSYS, Inc.). The SPIV velocity measurements acquired at the phantom inlet was applied as the inlet boundary condition.

Analysis

Because the sampling of the flow by the two methods were performed at different time points within a cardiac cycle, the SPIV-derived flow waveforms were interpolated in time using MATLAB cubic spline fitting (The MathWorks) before comparison with corresponding PC-MRI-derived flow waveforms. Correlation coefficients (R) and linear regression were used to compare the steady and pulsatile flow rates derived from conventional PC-MRI and SPIV techniques.

Flow rate error relative to SPIV measurements was calculated for each of the three phantom locations. Relative root mean squared error (RRMSE) was calculated according to:

$$RRMSE = \sqrt{\frac{\sum_t (f_{MRI}(t) - f_{SPIV}(t))^2}{\sum_t (f_{SPIV}(t))^2}} \quad [1]$$

where f is the flow measurement by either method and the summation is performed over different time points (40 measurements for pulsatile flows).

RESULTS

SPIV Reproducibility

SPIV provided a robust measurement of flow for both steady and pulsatile cases. In repeat experiments, the coefficient of variation, defined as the standard deviation divided by the mean, was less than 0.5% for steady flows and less than 1.5% for every time-point measurement in pulsatile flows determined over multiple cardiac cycles. In pulsatile flows, the programmed and measured flow waveforms differed

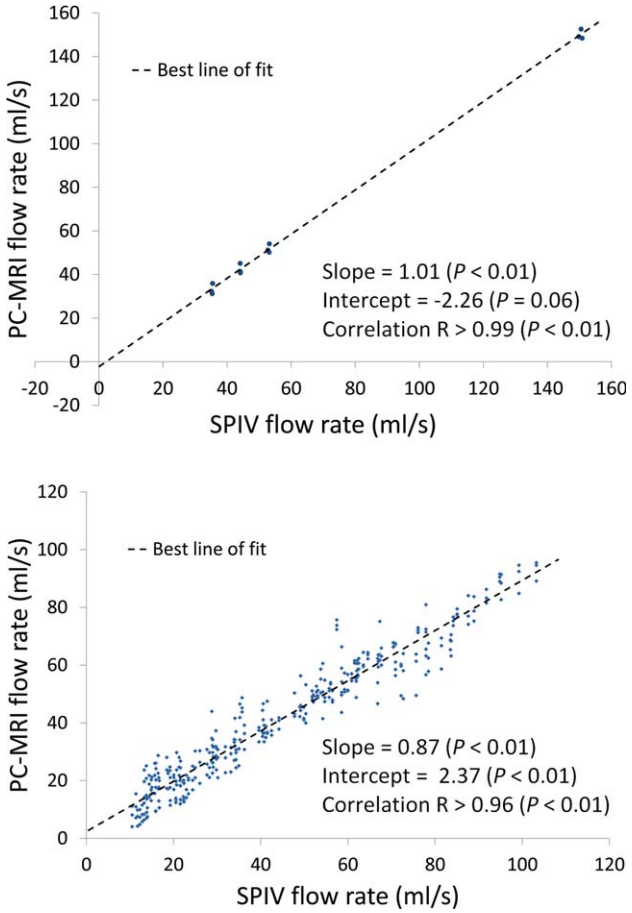

Figure 4. Scatter diagrams comparing conventional PC-MRI with SPIV flow measurements. Data for all flow regimes at the inlet of the three phantoms are combined in this plot. **a:** Steady flow (N = 12). **b:** Pulsatile flow (N = 360). [Color figure can be viewed in the online issue, which is available at wileyonlinelibrary.com.]

significantly due to the damping caused by the elastic connecting tubes. This leads to a delay and smoothing of the input waveform at the inlet of the phantom (Fig. 3). However, the total actual flow per cycle per minute remained unchanged.

Correlation of SPIV and Conventional PC-MRI Measurements at Inlet

Comparison of the flow measured by conventional PC-MRI and SPIV at the inlet of the three phantoms, where flow was fully developed, gives an estimate of the validity of PC-MRI for laminar flows. Results show good agreement between the two methods. The regression line approaches the line of identity with $f_{MRI} = 1.01\ f_{SPIV} - 2.26$ mL/s ($R > 0.99$) for steady flows (Fig. 4a). In pulsatile flows (Fig. 4b), this correlation can be expressed as: $f_{MRI} = 0.87\ f_{SPIV} + 2.37$ mL/s ($R > 0.96$) (with 40 samples per waveform).

Steady PC-MRI Measurement at Three Sections

Errors (difference in mean values) for steady flow measurements using conventional PC-MRI are reported in Table 2. All comparisons are based on SPIV as ground truth. For SF-0 and SF-1 flows, which benefit from suitable V_{enc} selection (3,26), the error at the inlet is less than 5%. Higher errors in SF-2 and SF-3 show the importance of choosing a proper V_{enc} (3,26).

Flow rate errors show that for the 87% and 74% stenoses, conventional PC-MRI underestimated flow at the outlet. For the same phantoms, flow measurements at both the inlet and the throat show very good agreement between the two methods. Through-plane velocity contours and profiles at the inlet for the 87% area occlusion phantom for flow SF-1 (see Table 1) are shown in Figure 5a. Both contour plots and velocity profiles show good agreement between the two methods.

Pulsatile PC-MRI Measurement at Three Sections

Flow waveforms measured by SPIV and gated, conventional PC-MRI at three sections for 50%, 74% and 87% phantoms and flows PF-1, PF-2, and PF-3 are shown in Figure 6a. The corresponding mean and peak flow errors as well as RRMSE are summarized in Table 3. While the mean flow measurement for the 50% stenosis phantom was relatively accurate at all three sections, for the other two phantoms the best accuracy was obtained at the throat. Also, conventional PC-MRI generally detected mean flow better than peak flow as evidenced by the smaller errors.

Through-plane velocity contours and profiles of pulsatile flow PF-1 for two time points t = 400 ms (corresponding to the maximum flow rate) and t = 275 ms (corresponding to the minimum flow rate) at the inlet are shown in Figure 5b and c for the 87% area occlusion phantom. Both contour plots and velocity profiles show good agreement between the methods. However, as V_{enc} was prescribed based on the maximum velocity in the flow, the near-wall velocities at t = 275 ms (Fig. 5c) were noisy.

Scatter diagrams comparing gated PC-MRI with SPIV flow measurements at three different sections for three different phantoms are shown in Figure 6b. Data for all flows PF-1, PF-2, and PF-3 were combined for each section/phantom in order to evaluate the accuracy of flow measurement as a function of imaging section. Correlation coefficients, slopes, and intercepts specific to each phantom model are summarized in

Table 2
Errors of the Steady Flow as Measured With PC-MRI Compared to SPIV

		Steady flow rate error (%)			
		SF-0	SF-1	SF-2	SF-3
87% Stenosis	Inlet	−1.6	−4.7	−7.6	−11.6
	Throat	−0.8	1.0	2.0	0.7
	Outlet	−4.6	−16.5	−22.2	−30.6
74% Stenosis	Inlet	−0.4	−2.8	−6.0	−7.8
	Throat	4.9	4.5	3.7	3.3
	Outlet	−3.4	−7.7	−10.0	−13.1
50% Stenosis	Inlet	1.4	1.8	2.4	1.2
	Throat	3.8	3.2	3.3	2.1
	Outlet	1.4	1.5	1.5	−1.3

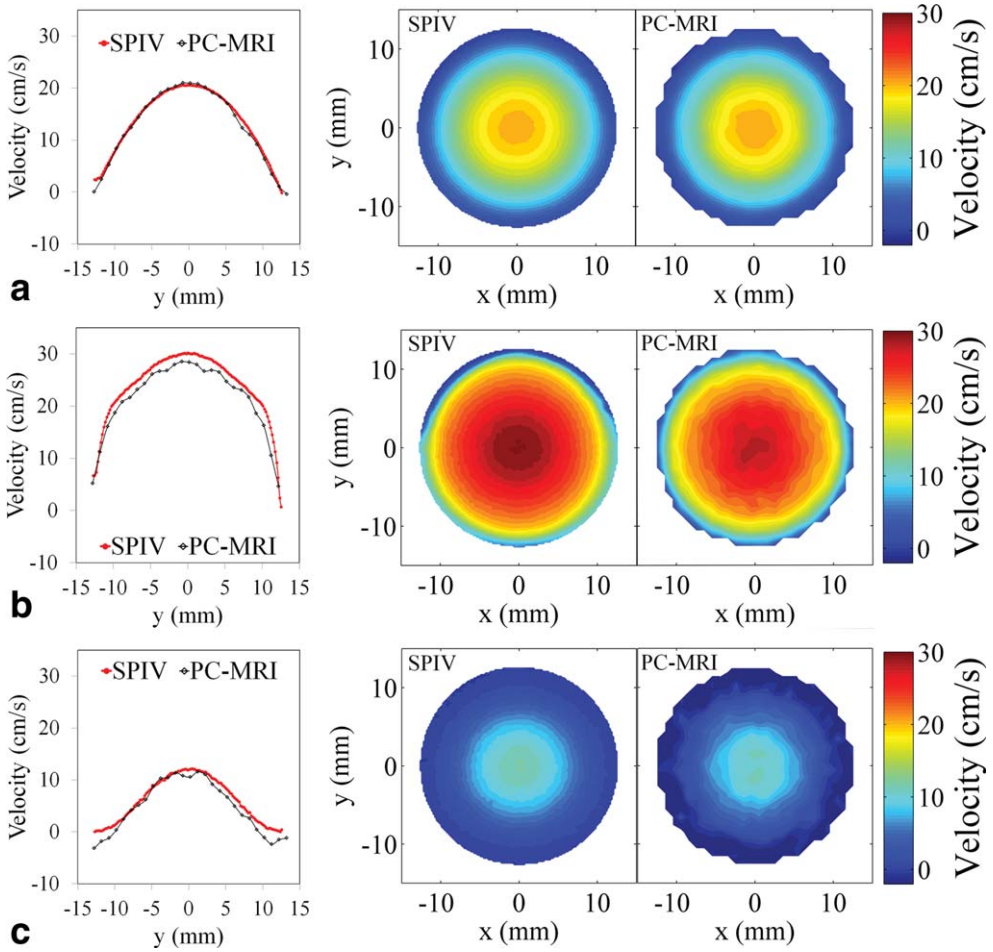

Figure 5. Through-plane velocity contours and profiles for steady and pulsatile flows at the inlet in the 87% area occlusion phantom: SF-1 (**a**), PF-1 (t = 400 ms; maximum flow) (**b**), and PF-1 (t = 275 ms; minimum flow) (**c**). Profiles are depicted for the cross line x = 0.

Table 3, showing good agreement between MRI and gold standard flow from SPIV.

Relative root mean squared error (RRMSE) for all phantoms, flows, and sections (Table 3) were higher compared with errors in mean flow measurement of the corresponding values in all cases. This may suggest decreased ability of the PC sequence which was used here to detect the high frequency components of the flow waveform.

DISCUSSION

To avoid long scan time and low signal-to-noise ratio, phase contrast measurements are usually performed at relatively low resolutions. This leads to a loss of flow information because of averaging of the velocity in a voxel, increased intravoxel dephasing, signal loss near vessel edges and inaccurate vessel wall definition as a result of partial volume effects. Furthermore, the phase velocity mapping technique assumes that velocity is constant over the measurement time, which introduces other sources of error to the measurements. Taking all these challenges into account before any clinical application, the accuracy of PC-MRI measurements, needs to be evaluated in phantom models for different pathologic conditions.

Our study provides an assessment of the accuracy of conventional PC-MRI flow measurements using an independent modality in a stenotic phantom of common iliac artery under both steady and pulsatile flow conditions, and presents a quantitative comparison between the two modalities. While the phantom hemodynamically recreates the idealized conditions of an iliac artery stenosis, the ratio of image resolution to artery dimension is not an accurate recreation. This leads to less pronounced partial volume errors which should be taken into account in in vivo cases.

In this study, we have shown that good qualitative and quantitative agreement exists between PC-MRI and SPIV measurements of flow patterns in phantom models of common iliac artery stenosis. For the Reynolds numbers that were studied, agreement was demonstrated for both steady and pulsatile measurements by evaluating the linear regression between the two methods, which showed a correlation coefficient of >0.99 and >0.96 for steady and pulsatile flows, respectively.

The difference between SPIV and PC-MRI measurements for steady flows with proper V_{enc} selection (SF-0 and SF-1) was less than 5% for both inlet and throat and showed good agreement in all cases. The agreement, however, was weaker at the outlet especially for the 87% stenosis. CFD simulations in Figure 7 have been used to spatially localize the source of error for steady flow SF-1. Comparison of the velocity contours at the outlet section fails to show any particular pattern explaining the errors associated with the higher flow rate. However, PC-MRI velocity contours at the outlet

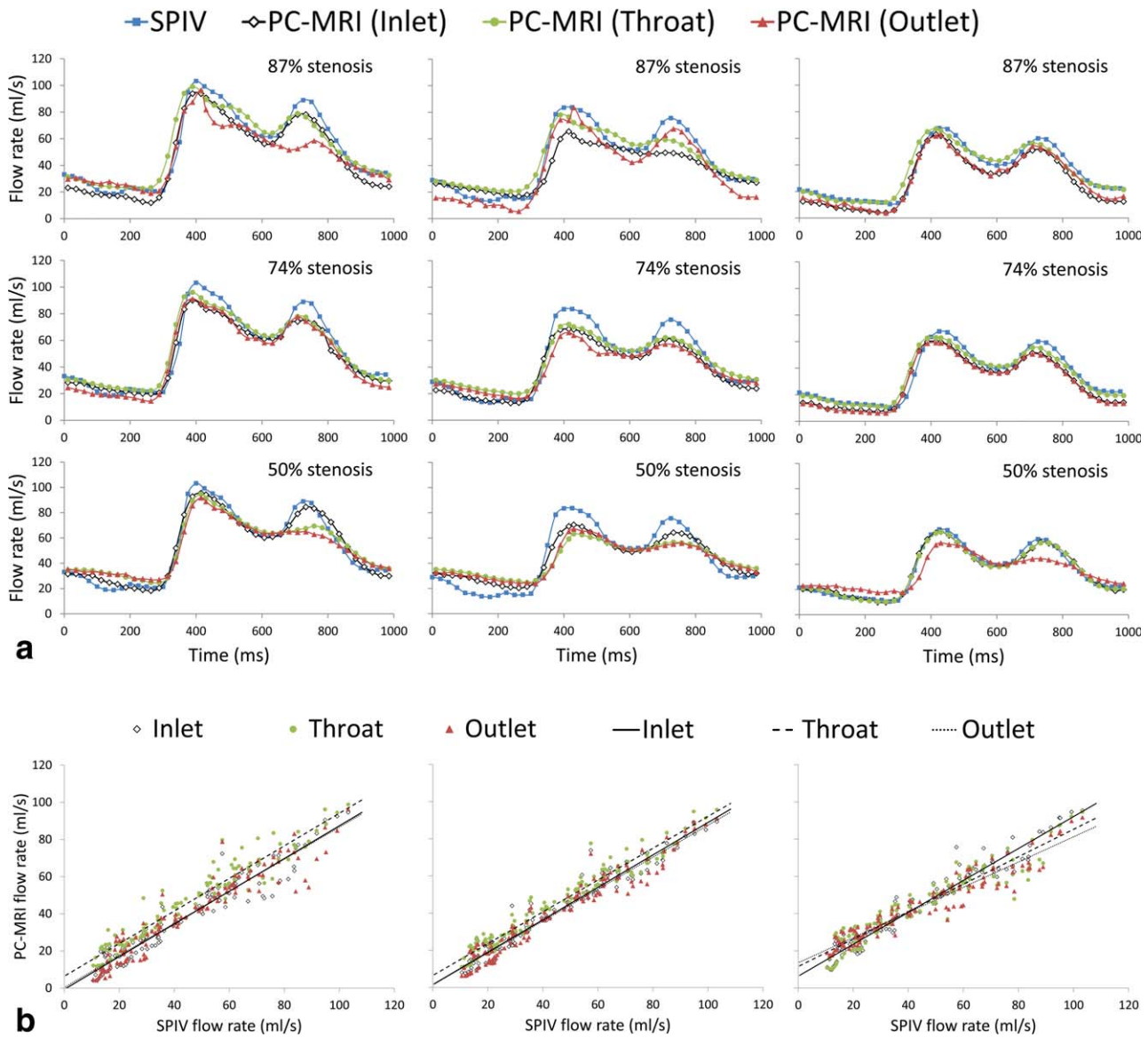

Figure 6. (a) Flow waveforms measured by SPIV and conventional PC-MRI at inlet, throat, and outlet. Top, middle, and bottom rows show results for 87%, 74% and 50% stenosis phantoms, respectively. Left, middle, and right columns show pulsatile flows PF-1, PF-2, and PF-3, respectively. (b) Scatter diagrams comparing conventional pulsatile PC-MRI with SPIV in the 90% (left), 75% (middle), and 50% (right) stenosis phantoms. Data for all flows PF-1, PF-2, and PF-3 are combined for each section/phantom (N = 120 for each section in each phantom). Solid, dashed, and dotted lines represent the best line of fit for inlet, throat, and outlet sections, respectively. Corresponding slopes, intercepts, and correlation coefficients specific to each phantom model are reported in Table 3.

are noisier compared with the other two sections. This may be explained by the fact that flow distal to the stenosis can be unsteady even in the constant flow cases (see for example (27)), causing spin dephasing. Flow measurement by each method assumes constant velocity over a short period of time. In the case of SF-1, this time period was 200 μs for SPIV (time difference between two consecutive images) and 3 ms for PC-MRI (time to collect data for the whole *k*-space was 256 msec). This time period is longer for pulsatile flows and/or when multiple signal averages are needed. At high flow rates, the longer the echo time, the higher the chance of intravoxel dephasing, fluid mixing, and flow artifacts distal to an occlusion. This longer time duration in conventional PC-MRI, due to more incoherent spin motion in the unsteady regions, may be viewed as introducing noise in the form of over/underestimation to the measured flow rates.

The same mechanism leads to errors in flow measurements of increasing magnitude in the distal section of more severe stenoses where flow unsteadiness is accentuated. Previous studies have shown an overestimation of flow by over 100% immediately upstream and downstream of the stenosis throat (18). However, compared with those studies, we used a reduced echo time to alleviate some of the problems associated with flow unsteadiness. For significant reduction, please see (29,30,31) and (14,15).

As seen in table 2, the steady flow errors for the SF-2 and SF-3 flow regimes also display more errors at

Table 3
Errors of the Mean and Peak Flow Measurements With Conventional PC-MRI for All Pulsatile Flows (Table 1)*

		Mean flow rate error (%)			Peak flow rate error (%)			RRMSE (%)			Linear correlation for all flows and (P values)		
		PF-1	PF-2	PF-3	PF-1	PF-2	PF-3	PF-1	PF-2	PF-3	Slope	Intercept	R
87% stenosis	Inlet	−10.4	−14.1	−19.2	−9.1	−21.7	−7.0	11.9	23.5	17.3	0.88 (<0.01)	−0.71 (0.52)	>0.96 (<0.01)
	Throat	2.3	1.16	1.5	−4.1	−6.7	−0.6	11.7	17.2	8.3	0.87 (<0.01)	6.39 (<0.01)	>0.96 (<0.01)
	Outlet	−10.8	−15.3	−15.3	−6.5	−0.2	−7.3	21.9	15.8	14.8	0.86 (<0.01)	0.32 (0.80)	>0.95 (<0.01)
74% stenosis	Inlet	−6.0	−11.4	−13.4	−12.7	−18.0	−11.3	11.5	16.5	14.3	0.87 (<0.01)	1.52 (0.09)	>0.97 (<0.01)
	Throat	0.42	−0.8	−1.0	−6.9	−13.8	−6.8	11.4	14.5	8.8	0.86 (<0.01)	6.41 (<0.01)	>0.97 (<0.01)
	Outlet	−8.8	−11.4	−15.5	−11.7	−21.0	−12.4	11.4	20.2	15.8	0.86 (<0.01)	1.36 (0.17)	>0.97 (<0.01)
50% stenosis	Inlet	0.3	−0.6	−0.9	−7.5	−15.7	−2.8	9.3	16.1	8.8	0.86 (<0.01)	6.31 (<0.01)	>0.97 (<0.01)
	Throat	0.9	−1.6	−1.4	−8.3	−24.3	−2.9	13.8	25.4	8.0	0.74 (<0.01)	11.50 (<0.01)	>0.94 (<0.01)
	Outlet	−1.6	−2.2	−2.9	−11.0	−19.5	−15.8	15.7	22.7	17.8	0.68 (<0.01)	13.50 (<0.01)	>0.95 (<0.01)

*Flow rates are compared against SPIV as the gold standard. RRMSE in addition to slope, intercept, and correlation coefficients (R) are also reported.

the outlet, though the errors were generally larger than those for the SF-0 and SF-1 waveforms. This originates from the well-known fact that velocity-to-noise ratio is proportional to V_{enc} (3,26) and proper V_{enc} selection in in vivo studies plays a crucial role in the accuracy of the measurements.

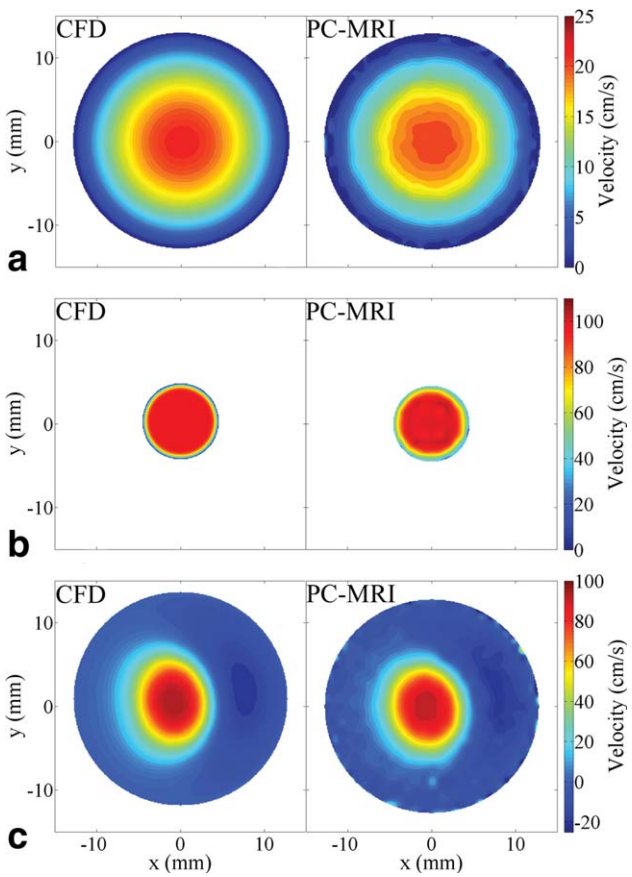

Figure 7. Through-plane velocity contours at three sections of the 87% stenosis phantom model: inlet (**a**), throat (**b**), and outlet (**c**) for steady flow SF-1.

The mean and peak flow rate errors, and RRMSE for all pulsatile flow regimens are reported in Table 3. For pulsatile flows, mean and peak flow rate errors were lowest at the throat section. This pattern, though less evident, was also observed in RRMSE. RRMSE was higher than error in the mean flow rate. Also, RRMSE for all phantoms, pulsatile flow regimes, and sections was found to be higher compared with steady flow for all cases, suggesting the decreased ability of the sequence to detect high frequency components of the flow waveform. Another factor that may have contributed to the observed results is that flow for inlet and outlet sections were measured off-center relative to the iso-center of the magnet. To address this limitation for future studies, it is recommended that all flow measurements be made at the iso-center.

As evident by the contour plots and profiles in Figure 5c, near-wall velocities at cardiac phases with low flow rates (e.g., t = 275 ms) are noisy, leading to underestimation of the flow for those cardiac phases. This occurs because in pulsatile studies, V_{enc} is generally set according to the peak flow rate and is kept constant over all cardiac phases. MR sequences with the capability to automatically optimize V_{enc} for individual heart phases in pulsatile flow could potentially prevent this underestimation (28).

In conclusion, SPIV is a robust and accurate in vitro method for 3D velocity and flow measurement with the ability to serve as the ground truth for PC-MRI velocity measurements. In particular, the approach taken here could serve as basis for validation and optimization of new and established MR velocimetry techniques. As shown by our measurements and statistical analyses, for the Reynolds numbers considered, at different sites

in the stenotic model and at different time instants, there is a good level of correspondence in flow measurement between conventional spin-warp PC-MRI with Cartesian read-out, and the SPIV method. The results reported here further supports the use of PC-MRI for studying stenotic flow behavior and suggests new avenues for research.

REFERENCES

1. Pelc NJ, Herfkens RJ, Shimakawa A, Enzmann DR. Phase contrast cine magnetic resonance imaging. Magn Reson Q 1991;7: 229–254.
2. Pelc NJ, Sommer FG, Li KC, Brosnan TJ, Herfkens RJ, Enzmann DR. Quantitative magnetic resonance flow imaging. Magn Reson Q 1994;10:125–147.
3. Nasiraei-Moghaddam A, Behrens G, Fatouraee N, Agarwal R, Choi ET, Amini AA. Factors affecting the accuracy of pressure measurements in vascular stenoses from phase-contrast MRI. Magn Reson Med 2004;52:300–309.
4. Frydrychowicz A, Stalder AF, Russe MF, et al. Three-dimensional analysis of segmental wall shear stress in the aorta by flow-sensitive four-dimensional-MRI. J Magn Reson Imaging 2009;30: 77–84.
5. Harloff A, Nussbaumer A, Bauer S, et al. In vivo assessment of wall shear stress in the atherosclerotic aorta using flow-sensitive 4D MRI. Magn Reson Med 2010;63:1529–1536.
6. Szolar DH, Sakuma H, Higgins CB. Cardiovascular applications of magnetic resonance flow and velocity measurements. J Magn Reson Imaging 1996;6:78–89.
7. Dambreville S, Chapman AB, Torres VE, et al. Renal arterial blood flow measurement by breath-held MRI: accuracy in phantom scans and reproducibility in healthy subjects. Magn Reson Med 2010;63:940–950.
8. Sondergaard L, Stahlberg F, Thomsen C, Stensgaard A, Lindvig K, Henriksen O. Accuracy and precision of MR velocity mapping in measurement of stenotic cross-sectional area, flow rate, and pressure gradient. J Magn Reson Imaging 1993;3:433–437.
9. Hoppe M, Heverhagen JT, Froelich JJ, Kunisch-Hoppe M, Klose KJ, Wagner HJ. Correlation of flow velocity measurements by magnetic resonance phase contrast imaging and intravascular Doppler ultrasound. Invest Radiol 1998;33:427–432.
10. Pelc LR, Pelc NJ, Rayhill SC, et al. Arterial and venous blood flow: noninvasive quantitation with MR imaging. Radiology 1992; 185:809–812.
11. Harloff A, Albrecht F, Spreer J, et al. 3D blood flow characteristics in the carotid artery bifurcation assessed by flow-sensitive 4D MRI at 3T. Magn Reson Med 2009;61:65–74.
12. Lee VS, Spritzer CE, Carroll BA, et al. Flow quantification using fast cine phase-contrast MR imaging, conventional cine phase-contrast MR imaging, and Doppler sonography: in vitro and in vivo validation. AJR Am J Roentgenol 1997;169:1125–1131.
13. Zananiri FV, Jackson PC, Halliwell M, et al. A comparative study of velocity measurements in major blood vessels using magnetic resonance imaging and Doppler ultrasound. Br J Radiol 1993;66: 1128–1133.
14. O'Brien KR, Cowan BR, Jain M, Stewart RA, Kerr AJ, Young AA. MRI phase contrast velocity and flow errors in turbulent stenotic jets. J Magn Reson Imaging 2008;28:210–218.
15. O'Brien KR, Myerson SG, Cowan BR, Young AA, Robson MD. Phase contrast ultrashort TE: a more reliable technique for measurement of high-velocity turbulent stenotic jets. Magn Reson Med 2009;62:626–636.
16. Hollnagel DI, Summers PE, Kollias SS, Poulikakos D. Laser Doppler velocimetry (LDV) and 3D phase-contrast magnetic resonance angiography (PC-MRA) velocity measurements: validation in an anatomically accurate cerebral artery aneurysm model with steady flow. J Magn Reson Imaging 2007;26:1493–1505.
17. Ku DN, Biancheri CL, Pettigrew RI, Peifer JW, Markou CP, Engels H. Evaluation of magnetic resonance velocimetry for steady flow. J Biomech Eng 1990;112:464–472.
18. Siegel JM Jr, Oshinski JN, Pettigrew RI, Ku DN. The accuracy of magnetic resonance phase velocity measurements in stenotic flow. J Biomech 1996;29:1665–1672.
19. Hollnagel DI, Summers PE, Poulikakos D, Kollias SS. Comparative velocity investigations in cerebral arteries and aneurysms: 3D phase-contrast MR angiography, laser Doppler velocimetry, and computational fluid dynamics. NMR Biomed 2009;22:795–808.
20. Kitajima HD, Sundareswaran KS, Teisseyre TZ, et al. Comparison of particle image velocimetry and phase contrast MRI in a patient-specific extracardiac total cavopulmonary connection. J Biomech Eng 2008;130:041004.
21. van Ooij P, Guedon A, Poelma C, et al. Complex flow patterns in a real-size intracranial aneurysm phantom: phase contrast MRI compared with particle image velocimetry and computational fluid dynamics. NMR Biomed 2012;25:14–26.
22. Frayne R, Holdsworth DW, Gowman LM, et al. Computer-controlled flow simulator for MR flow studies. J Magn Reson Imaging 1992;2:605–612.
23. Shakeri M, Khodarahmi I, Sharp MK, Amini AA. Optical imaging of steady flow in a phantom model of iliac artery stenosis: comparison of CFD simulations with PIV measurements. In: Proceedings of SPIE, San Diego, 2010. (abstract 76260L).
24. Khodarahmi I, Shakeri M, Sharp M, Amini AA. Using PIV to determine relative pressures in a stenotic phantom under steady flow based on the Pressure-Poisson equation. Conf Proc IEEE Eng Med Biol Soc 2010;1:2594–2597.
25. van Doorne C, Westerweel J. Measurement of laminar, transitional, and turbulent pipe flow using Stereoscopic-PIV. Exp Fluids 2007;42:259–279.
26. Gudbjartsson H, Patz S. The Rician distribution of noisy MRI data. Magn Reson Med 1995;34:910–914.
27. Griffith MD, Leweke T, Thompson MC, Hourigan K. Steady inlet flow in stenotic geometries: convective and absolute instabilities. J Fluid Mech 2008;616:111–133.
28. Ringgaard S, Oyre SA, Pedersen EM. Arterial MR imaging phase-contrast flow measurement: improvements with varying velocity sensitivity during cardiac cycle. Radiology 2004;232:289–294.
29. Kadbi M, Wang H, Warner L, Traughber M, Alshaher M, Yancey A, Heidenreich J, Amini A. 3D Cine Ultra-short TE (UTE) Phase Contrast Imaging in Carotid Arteries: Comparison with Conventional Technique. International Society of Magnetic Resonance in Medicine, Melbourne, Australia, May 2012.
30. Kadbi M, Negahdar MJ, Cha J, Traughber M, Martin P, Amini A. Validation of 3D Ultra-Short TE (UTE) Phase-Contrast MRI For Imaging of Steady Flow: Initial Phantom Experiments. IEEE Engineering in Medicine and Biology Conference, San Diego, CA, September 2012.
31. Kadbi M, Traughber M, Martin P, Amini A. 4D UTE Flow: A Novel 4D Ultra-Short TE Phase-Contrast MRI Technique for Assessment of Flow and Hemodynamics. International Society for Magnetic Resonance in Medicine, Salt Lake City, Utah, April 2013.